Fabrication and Transport Properties of Single-Molecule-Thick Electrochemical Junctions

Eric W. Wong, Charles P. Collier, Martin Běhloradský, Françisco M. Raymo, J. Fraser Stoddart,* and James R. Heath*

Contribution from the Department of Chemistry and Biochemistry, University of California, Los Angeles, 405 Hilgard Avenue, Los Angeles, California 90095-1569

Received November 2, 1999

Abstract: A V-shaped compound incorporating two bipyridinium units, which emanate from a central hydrophilic core and bear hydrophobic tetraarylmethane-based stoppers at each end, was designed and synthesized. In a thermodynamically controlled self-assembly process in solution, either one or two 1,4-dioxybenzene-based macrocyclic polyethers can be slipped over the bulky stoppers of the V-shaped compound, affording either a [2]rotaxane or a [3]rotaxane, respectively. The parent V-shaped compound and the two rotaxanes incorporate two redox-active bipyridinium units that can be reduced reversibly and two redox-active phenoxy groups in the stoppers that can be oxidized irreversibly. Furthermore, these three compounds have amphiphilic character and, as a result, form stable monolayers at the air/water interface. Langmuir−Blodgett monolayers of these compounds were sandwiched between two electrodes to afford molecule-based solid-state switches. In forward bias mode, the $I-V$ characteristics of the junction are reversible, but upon application of a sufficient reverse bias the junction resistance is irreversibly decreased, thereby switching the device. As a result, the current flowing through the device at forward bias voltages is lowered by a factor of 60−80. The behavior of the solid-state devices can be interpreted on the basis of the redox properties determined in solution for the three compounds. Initially, current flow at forward bias is determined by resonant tunneling through the molecular LUMO states associated with the bipyridium units. The irreversible decrease in current that occurs at reverse biases suggests a similarity to the solution-phase oxidation of the phenoxy groups.

Introduction

The field of molecular electronics[1] began nearly 30 years ago when Aviram and Ratner[2] proposed the concept of molecular rectifiers. Since that time, advances in synthetic supramolecular chemistry,[3] coupled with recent developments in device fabrication technologies[4] and scanning probe methods,[5] have brought molecular electronics to the point where single molecules have been manipulated, imaged, and investigated electronically.[6c,f,7a] The attraction of molecular electronics is that synthetic chemistry is mature enough to offer innumerably different molecular structures with differing electronic properties. A challenge has been to understand and design electronic properties of molecules that determine the properties of a device. Scanning tunneling microscopy has revealed that molecules retain their basic molecular electronic identities on surfaces.[7] Solid-state devices composed of monolayers or single-molecule junctions have displayed diode and rectifying behavior associated with the

(1) (a) *Molecular Electronic Devices*; Carter, F. L., Ed.; Dekker: New York, 1982. (b) *Molecular Electronic Devices*; Carter, F. L., Ed.; Dekker: New York, 1987. (c) *Molecular Electronic Devices*; Carter, F. L., Siatkowski, R. E., Wohltgen, H., Eds.; Elsevier: Amsterdam, 1988. (d) *Molecular Electronics—Science and Technology*; Aviram, A., Ed.; Engineering Foundation: New York, 1989. (e) *Molecular Electronics: Materials and Methods*; Lazarev, P. I., Ed.; Kluwer Academic Publishers: Dordrecht, 1991. (f) *Molecular Electronics—Science and Technology*; Aviram, A., Ed.; American Institute of Physics: Washington, 1992. (g) *Molecular Electronics*; Ashwell, G. J., Ed.; Wiley: New York, 1992. (h) *Molecular Electronics and Molecular Electronic Devices*; Sienicki, K., Ed.; CRC Press: Boca Raton, FL, 1993. (i) *Molecular and Biomolecular Electronics;* Birge, R. R., Ed.; American Chemical Society, Washington, DC, 1994. (j) *Introduction to Molecular Electronic Devices*; Petty, M. C., Bryce, M. R., Bloor, D., Eds.; Oxford University Press: New York, 1995. (k) *Molecular Electronics*; Jortner, J., Ratner, M., Eds.; Blackwell Science: Oxford, 1997. (l) *Molecular Electronics: Science and Technology*; Aviram, A., Ratner, M., Eds.; New York Academy of Sciences: New York, 1998.

(2) Aviram, A.; Ratner, M. A. *Chem. Phys. Lett.* **1974**, *29*, 277−283.

(3) Fyfe, M. C. T.; Stoddart, J. F. *Acc. Chem. Res.* **1997**, *30*, 393−401.

(4) (a) Moreau, W. M. *Semiconductor Lithography: Principles and Materials*; Plenum Press: New York, 1988. (b) *Lithography in Microelectronics*; Makhviladze, T. M., Ed.; Nova Science Publishers: Commack, NY, 1989. (c) *Nanolithography: a Borderland between STM, EB, IB, and X-ray Lithographies*; Gentili, M., Giovannella, C., Selci, S., Eds.; Kluwer Academic Publishers: Dordrecht, 1994. (d) Levinson, H. J. *Lithography Process Control*; Optical Engineering Press: Bellingham, WA, 1999.

(5) (a) *Scanning Tunneling Microscopy and Related Methods*; Behm, R. J., Garcia, N., Rohrer, H., Eds.; Kluwer Academic Publishers: Dordrecht, 1990. (b) Wiesendanger, R. *Scanning Probe Microscopy and Spectroscopy: Methods and Applications*; Cambridge University Press: Cambridge, 1994. (c) *Scanning Probe Microscopy: Analytical Methods*; Wiesendanger, R., Ed.; Springer-Verlag: Berlin, 1998.

(6) (a) Hipps, K. W.; Mazur, U. *J. Phys. Chem.* **1994**, *98*, 5824−5829. (b) Burghard, M.; Fischer, C. M.; Roth, S.; Schlick, U.; Hanack, M. *Synth. Met.* **1996**, *76*, 241−244. (c) Klein, D. L.; McEuen, P. L.; Katari, J. E. B.; Roth, R.; Alivisatos, A. P. *Appl. Phys. Lett.* **1996**, *68*, 2574−2576. (d) Roth, S.; Blumentritt, S.; Burghard, M.; Fischer, C. M.; Philipp, G.; Müller-Schwanneke, C. *Synth. Met.* **1997**, *86*, 2415−2418. (e) Metzger, R. M.; Chen, B.; Höpfner, U.; Lakshmikantham, M. V.; Vuillaume, D.; Kawai, T.; Wu, X.; Tachibana, H.; Hughes, T. V.; Sakurai, H.; Baldwin, J. W.; Hosch, C.; Cava, M. P.; Brehmer, L.; Ashwell, G. J. *J. Am. Chem. Soc.* **1997**, *119*, 10455−10466. (f) Reed, M. A.; Zhou, C.; Muller, C. J.; Burgin, T. P.; Tour, J. M. *Science* **1997**, *278*, 252−254. (g) Zhou, C.; Deshpande, M. R.; Reed, M. A.; Jones, L., II; Tour, J. M. *Appl. Phys. Lett.* **1997**, *71*, 611−613.

(7) (a) Joachim, C.; Gimzewski, J. K.; Schlittler, R. R.; Chavy, C. *Phys. Rev. Lett.* **1995**, *74*, 2102−2105. (b) Ottaviano, L.; Santucci, S.; Di Nardo, S.; Lozzi, L.; Passacantando, M.; Picozzi, P. *J. Vac. Sci. Technol. A* **1997**, *15*, 1014−1019. (c) Datta, S.; Tian, W.; Hong, S.; Reifenberger, R.; Henderson, J. I.; Kubiak, C. P. *Phys. Rev. Lett* **1997**, *79*, 2530−2533.

10.1021/ja993890v CCC: $19.00
Published on Web 05/31/2000

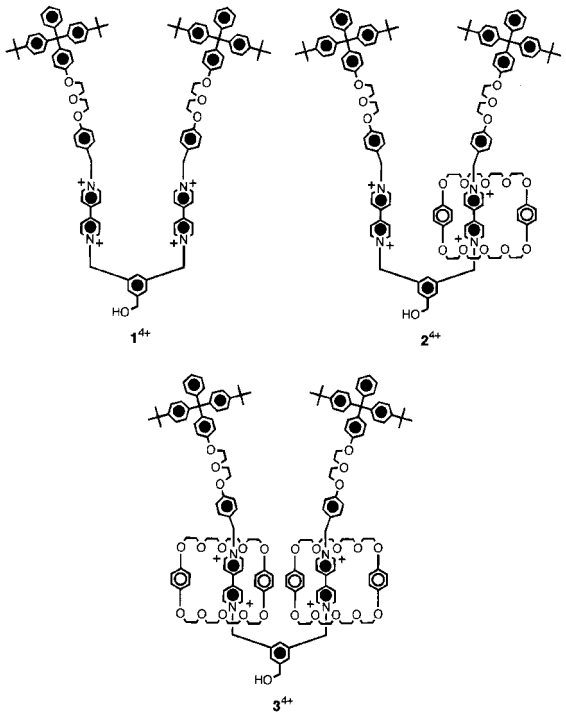

Figure 1. Doubly branched V-shaped compound $\mathbf{1}^{4+}$, [2]rotaxane $\mathbf{2}^{4+}$, and [3]rotaxane $\mathbf{3}^{4+}$.

molecular electronic states.[6,8,9] In this paper we report on molecule-based, solid state, singly configurable switches fabricated from molecules designed to incorporate specific redox behavior as well as self-assembly properties utilized in the device fabrication. We will describe (1) the synthesis of some redox-active amphiphilic compounds, two of which are rotaxanes,[3] (2) the fabrication of devices with these compounds, and (3) the properties of the devices in which a single-molecule-thick electrochemical cell is sandwiched between two metal electrodes. We outline a synthesis of the redox-active compounds, which involves a thermodynamically controlled approach[3] to the self-assembly of the rotaxanes. We describe a device fabrication procedure that is relatively simple and inexpensive and produces reliable devices in high yield. This procedure allows us to fabricate many devices in parallel and to accumulate meaningful statistics on the transport properties of these devices. It also allows us to incorporate a variety of different electrode combinations and different molecules into our devices, and to investigate systematically molecular structure/device property relationships. We compare and contrast the current/voltage characteristics of these devices with solution-phase voltammetry measurements. In a forthcoming paper, a phenomenological model for these devices will be presented and correlated to the results from solution-phase voltammetry.

The compounds utilized in this work are illustrated in Figure 1. The current−voltage characteristics of tunnel junctions fabricated from eicosanoic acid and similar linear amphiphilic molecules were previously reported by Kuhn[8a] and Sagiv.[8b] As a first check, we have made certain that when we incorporate eicosanoic acid into our devices, we reproduce the results

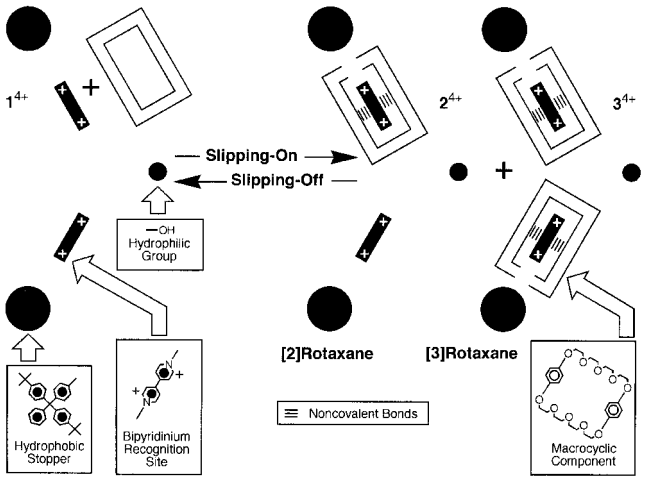

Figure 2. Design and synthetic strategy for the construction of amphiphilic rotaxanes.

reported previously. The molecules shown in Figure 1 are the V-shaped compounds $\mathbf{1}^{4+}$ and the [2]rotaxane $\mathbf{2}^{4+}$ and the [3]-rotaxane $\mathbf{3}^{4+}$ derived from it. Although the details of the voltammetry measurements vary somewhat from molecule to molecule, all three of these molecular systems may be reduced reversibly and oxidized *irreversibly* at relatively low voltages.

The key to the success of our devices is the careful design of molecules that (1) form monolayers of sufficient quality to make metal−monolayer−metal sandwich structures, (2) contain the appropriate units to enable resonant tunneling as well as switching, and (3) have functionality that can withstand deposition of a metal, while protecting electroactive portions of the molecules.

Design and Synthetic Strategy

We have demonstrated[10] that bipyridinium-containing catenanes and rotaxanes can be introduced into Langmuir films and Langmuir−Blodgett multilayers. In particular, we have shown[10c] that amphiphilic [*n*]rotaxanes, having a positively charged bipyridinium core with appended tetraarylmethane groups, form stable monolayers at the air/water interface. The hydrophilic bipyridinium core lies on the water surface, while the hydrophobic tetraarylmethane groups stand away from it. These observations suggested the design of amphiphilic rotaxanes (Figure 2) composed of a V-shaped component with two arms, each terminated by a hydrophobic tetraarylmethane group, and a hydrophilic group at their junction. In addition to imposing amphiphilic character on the rotaxane, the bulky tetraarylmethane groups mechanically trap the macrocyclic component(s). These amphiphilic rotaxanes can be assembled using a well-established synthetic strategy—namely, the so-called slipping approach.[11] This thermodynamically controlled self-assembly[12] procedure relies on the size-complementarity between the cavity of the macrocyclic component(s) and the stoppers. When a solution of an appropriate macrocycle and a complementary V-shaped compound containing two recognition sites is heated, the macrocycle slips over one of the stoppers of the V-shaped

(8) (a) Mann, B.; Kuhn, H. *J. Appl. Phys.* **1971**, *42*, 4398−4405. (b) Polymeropoulos, E. E.; Sagiv, J. *J. Chem. Phys.* **1978**, *69*, 1836−1847.

(9) For reviews of molecular electronic and other nanoelectronic devices, see: (a) Goldhaber-Gordon, D.; Montermerlo, S.; Love, J. C.; Opiteck, G. J.; Ellenbogen, J. C. *Proc. IEEE-Int. Soc. Opt. Eng.* **1997**, *85*, 521−540. (b) Aviram, A. *Int. J. Quantum Chem.* **1992**, *42*, 1615−1624. (c) Simon, J.; Tournilhac, F. *New J. Chem.* **1987**, 11, 383−399. (d) Ulman, A. *Introduction to Ultrathin Organic Films: from Langmuir−Blodgett to Self-Assembly*; Academic Press: Boston, 1991.

(10) (a) Ahuja, R. C.; Caruso, P.-L.; Möbius, D.; Wildburg, G.; Ringsdorf, H.; Philp, D.; Preece, J. A.; Stoddart, J. F. *Langmuir* **1993**, *9*, 1534−1544. (b) Ahuja, R. C.; Caruso, P.-L.; Möbius, D.; Philp, D.; Preece, J. A.; Ringsdorf, H.; Stoddart, J. F.; Wildburg, G. *Thin Solid Films* **1996**, *284/285*, 671−677. (c) Amabilino, D. B.; Asakawa, M.; Ashton, P. R.; Ballardini, R.; Balzani, V.; Belohradsky, M.; Credi, A.; Higuchi, M.; Raymo, F. M.; Shimizu, T.; Stoddart, J. F.; Venturi, M.; Yase, K. *New J. Chem.* **1998**, 959−972. (d) Brown, C. L.; Jonas, U.; Preece, J. A.; Ringsdorf, H.; Seitz, M.; Stoddart, J. F. *Langmuir* **2000**, *16*, 1924−1930.

component, affording a mixture of rotaxanes. The opposing process—namely, slipping-off of the macrocyclic component—also occurs at high temperatures. Thus, an equilibrium between the separate components and the rotaxanes is eventually established. This equilibrium lies in favor of the rotaxanes since they are stabilized, relative to the separate components, by noncovalent bonding interactions between the π-electron-deficient bipyridinium recognition sites and the π-electron-rich macrocyclic polyether. Upon cooling of the solution to ambient temperature, the slipping processes slow significantly. As a result, the rotaxanes become kinetically stable and can be separated by column chromatography.

In the rotaxanes, the encircled bipyridinium recognition sites are sandwiched between the two 1,4-dioxybenzene rings of the macrocyclic components. The associated [$\pi\cdots\pi$] stacking interactions are supplemented by [C—H$\cdots$O] hydrogen bonds between the α-bipyridinium hydrogen atoms and the polyether oxygen atoms. The recognition properties of a bipyridinium unit, however, are "switched off" upon its reduction. Indeed, the monoelectronic reduction of a dicationic bipyridinium unit produces a radical monocation that can be reduced further by the addition of a second electron. Both reduction processes are reversible and can be easily achieved electrochemically. The redox properties of the bipyridinium units incorporated with pseudorotaxanes and catenanes have been exploited to control reversibly the relative movements of their components, paving the way for the realization of molecular-sized switches and logic gates.[13]

Experimental Section

Synthesis. Solvents were purchased from Aldrich and purified according to literature procedures.[14] Reagents were purchased from Aldrich except for **4**,[15] **7**[11a] (Scheme 1), and **8**[16] (Scheme 2), which were synthesized according to literature procedures. Thin-layer chromatography (TLC) was carried out using aluminum sheets, precoated with silica gel 60F (Merck 5554) or aluminum oxide $60F_{254}$ neutral (Merck 5550). The plates were inspected by using UV light prior to development with iodine vapor. Melting points were determined on an Electrothermal 9200 apparatus and are uncorrected. Liquid secondary ion mass spectra (LSIMS) were recorded on a VG Zabspec triple-focusing mass spectrometer. ^{1}H NMR and ^{13}C NMR spectra were recorded on a Bruker AC300 (300 and 75 MHz, respectively) spectrometer. All chemical shifts are quoted in ppm on the δ scale using TMS or the solvent as the internal standard. Elemental analyses were performed by Quantitative Technologies Inc.

Scheme 1

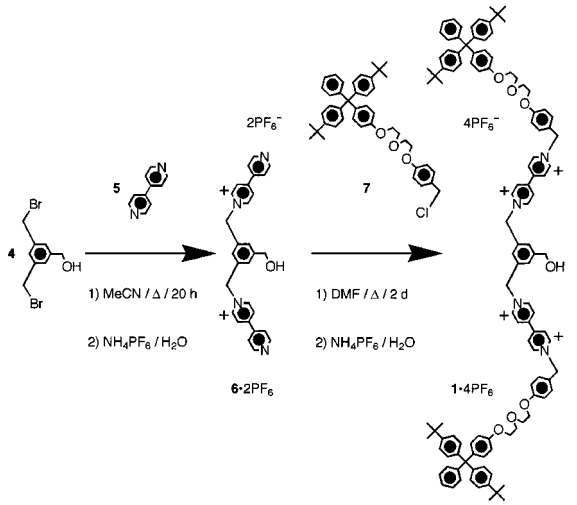

Scheme 2

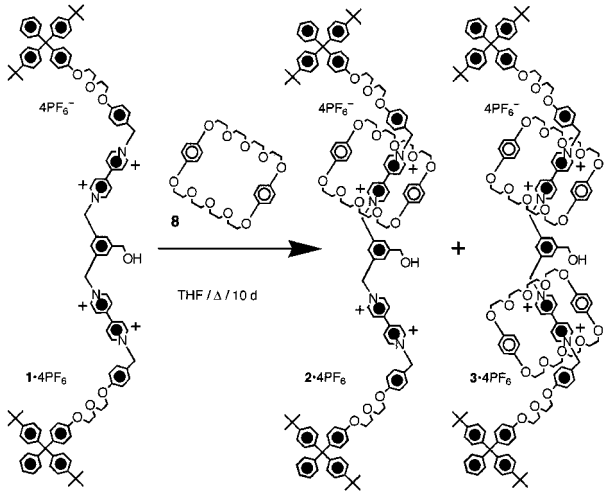

(i) Bis(hexafluorophosphate) Salt 6·2PF$_6$. A solution of **4** (3.5 g, 12 mmol) in MeCN (50 mL) was added over 30 min to a solution of 4,4′-bipyridine (**5**) (10 g, 64 mmol) in MeCN (150 mL) heated under reflux and an atmosphere of Ar. The mixture was heated under reflux for an additional 20 h. After the mixture cooled to ambient temperature, Et_2O (1 L) was added. The resulting precipitate was filtered off, washed with Et_2O (1 L), and dissolved in H_2O (1 L). After the addition of NH_4PF_6 (16 g, 100 mmol), a white solid precipitated out. The solid was filtered off, washed with H_2O (2 L), and dried to afford **3**·2PF$_6$ (9.8 g, 92%) as a white solid. Mp: >250 °C. LSIMS: *m*/*z* = 591 [M − PF$_6$]$^+$, 446 [M − 2PF$_6$]$^+$. ^{1}H NMR [$(CD_3)_2CO$]: δ = 9.41 (4H, d, J = 7 Hz), 8.96 (4H, d, J = 6 Hz), 8.76 (4H, d, J = 7 Hz), 8.05 (4H, d, J = 6 Hz), 7.96 (1H, s), 7.82 (2H, s), 6.21 (4H, s), 4.78 (2H, s). Anal. Calcd for $C_{29}H_{26}F_{12}N_4OP_2$: C = 47.30, H = 3.56, N = 7.61. Found: C = 47.22, H = 3.60, N = 7.58.

(11) (a) Ashton, P. R.; Ballardini, R.; Balzani, V.; Belohradsky, M.; Gandolfi, M. T.; Philp, D.; Prodi, L.; Raymo, F. M.; Reddington, M. V.; Spencer, N.; Stoddart, J. F.; Venturi, M.; Williams, D. J. *J. Am. Chem. Soc.* **1996**, *118*, 4931−4951. (b) Asakawa, M.; Ashton, P. R.; Ballardini, R.; Balzani, V.; Belohradsky, M.; Gandolfi, M. T.; Kocian, O.; Prodi, L.; Raymo, F. M.; Stoddart, F. M.; Venturi, M. *J. Am. Chem. Soc.* **1997**, *119*, 302−310. (c) Raymo, F. M.; Stoddart, J. F. *Pure Appl. Chem.* **1997**, *69*, 1987−1997. (d) Ashton, P. R.; Baxter, I.; Fyfe, M. C. T.; Raymo, F. M.; Spencer, N.; Stoddart, J. F.; White, A. J. P.; Williams, D. J. *J. Am. Chem. Soc.* **1998**, *120*, 2297−2307. (e) Raymo, F. M.; Houk, K. N.; Stoddart, J. F. *J. Am. Chem. Soc.* **1998**, *120*, 9318−9322.

(12) (a) Philp, D.; Stoddart, J. F. *Synlett* **1991**, 445−458. (b) Amabilino, D. B.; Stoddart, J. F. *Chem. Rev.* **1995**, *95*, 2725−2828. (c) Philp, D.; Stoddart, J. F. *Angew. Chem., Int. Ed. Engl.* **1996**, *35*, 1154−1196. (d) Gillard, R. E.; Raymo, F. M.; Stoddart, J. F. *Chem. Eur. J.* **1997**, *3*, 1933−1940. (e) Raymo, F. M.; Stoddart, J. F. *Chemtracts−Org. Chem.* **1998**, *11*, 491−511. (f) Raymo, F. M.; Stoddart, J. F. *Chem. Rev.* **1999**, *99*, 1643−1663.

(13) For examples of bipyridinium-based switches and logic gates, see: (a) Anelli, P.-L.; Asakawa, M.; Ashton, P. R.; Bissell, R. A.; Clavier, G.; Górski, R.; Kaifer, A. E.; Langford, S. J.; Mattersteig, G.; Menzer, S.; Philp, D.; Slawin, A. M. Z.; Spencer, N.; Stoddart, J. F.; Tolley, M. S.; Williams, D. J. *Chem. Eur. J.* **1997**, *3*, 1113−1135. (b) Asakawa, M.; Ashton, P. R.; Balzani, V.; Credi, A.; Mattersteig, G.; Matthews, O. A.; Montalti, M.; Spencer, N.; Stoddart, J. F.; Venturi, M. *Chem. Eur. J.* **1997**, *3*, 1992−1996. (c) Credi, A.; Balzani, V.; Langford, S. J.; Stoddart, J. F. *J. Am. Chem. Soc.* **1997**, *119*, 2679−2681. (d) Ashton, P. R.; Balzani, V.; Becher, J.; Credi, A.; Fyfe, M. C. T.; Mattersteig, G.; Menzer, S.; Nielsen, M. B.; Raymo, F. M.; Stoddart, J. F.; Venturi, M.; White, A. J. P.; Williams, D. J. *J. Am. Chem. Soc.* **1999**, *121*, 3951−3957. (e) Balzani, V.; Credi, A.; Mattersteig, G.; Matthews, O. A.; Raymo, F. M.; Stoddart, J. F.; Venturi, M.; White, A. J. P.; Williams, D. J. *J. Org. Chem.* **2000**, *65*, 1924−1936.

(14) Perrin, D. D.; Armarego, W. L. *Purification of Laboratory Chemicals*, 3rd ed.; Pergamon Press: New York, 1988.

(15) Menzer, S.; White, A. J. P.; Williams, D. J.; Belohardsky, M.; Hamers, C.; Raymo, F. M.; Shipway, A. N.; Stoddart, J. F. *Macromolecules* **1998**, *31*, 295−307.

(16) Anelli, P.-L.; Ashton, P. R.; Ballardini, R.; Balzani, V.; Delgado, M.; Gandolfi, M. T.; Goodnow, T. T.; Kaifer, A. E.; Philp, D.; Pietraszkiewicz, M.; Prodi, L.; Reddington, M. V.; Slawin, A. M. Z.; Spencer, N.; Stoddart, J. F.; Vicent, C.; Williams, D. J. *J. Am. Chem. Soc.* **1992**, *114*, 193−218.

(ii) Tetrakis(hexafluorophosphate) Salt 1·4PF$_6$. A solution of **7** (10 g, 15 mmol) in DMF (500 mL) and **6**·2PF$_6$ (4.2 g, 6 mmol) was heated at 70 °C for 2 d under an atmosphere of Ar. After the solution cooled to ambient temperature, the solvent was distilled off under reduced pressure, and the residue was washed with Et_2O (1 L) and dissolved in H_2O (1 L). After the addition of NH_4PF_6 (20 g, 123 mmol), a white solid precipitated out. The solid was filtered off, washed with H_2O (2 L), and dried to afford **1**·4PF$_6$ (12.6 g, 97%) as a white solid. Mp: >250 °C. LSIMS: *m*/*z* = 2133 [M − PF$_6$]$^+$, 1988 [M − 2PF$_6$]$^+$, 1843 [M − 3PF$_6$]$^+$, 1698 [M − 4PF$_6$]$^+$. ^{1}H NMR [$(CD_3)_2CO$]: δ = 9.44 (4H, d, J = 7 Hz), 9.38 (4H, d, J = 7 Hz), 8.76−8.68 (8H, m), 7.78 (1H, s), 7.76 (2H, s), 7.51 (4H, d, J = 9 Hz), 7.34−7.04 (34H, m), 6.84 (4H, d, J = 9 Hz), 6.16 (4H, s), 6.10 (4H, s), 4.69 (2H, s), 4.30−4.05 (8H, m), 3.96−3.80 (8H, m), 1.29 (36H, s). Anal. Calcd for $C_{117}H_{124}F_{24}N_4O_7P_4$: C = 61.69, H = 5.49, N = 2.46. Found: C = 61.42, H = 5.52, N = 2.44.

(iii) [2]Rotaxane 2·4PF$_6$ and [3]Rotaxane 3·4PF$_6$. A solution of **5**·4PF$_6$ (2.3 g, 1 mmol) and bis-*p*-phenylene-34-crown-10 (**8**) (10.0 g, 19 mmol) in THF (200 mL) was heated at 55 °C for 10 d under an atmosphere of Ar. After the solution cooled to ambient temperature, the solvent was distilled off under reduced pressure, and the residue was purified by column chromatography [SiO_2:Me_2CO/hexane (3:2) and then 5 mM NH_4PF_6 in Me_2CO]. The resulting two products were washed individually with H_2O (1 L) and dried to afford, in order of elution, **3**·4PF$_6$ (1.75 g, 52%) and **2**·4PF$_6$ (0.38 g, 14%) as red solids. Data for **3**·4PF$_6$ follow. Mp: >250 °C. LSIMS: *m*/*z* = 2669 [M − PF$_6$]$^+$, 2524 [M − 2PF$_6$]$^+$, 2379 [M − 3PF$_6$]$^+$, 2234 [M − 4PF$_6$]$^+$. ^{1}H NMR [$(CD_3)_2CO$]: δ = 9.28 (8H, d, J = 7 Hz), 8.47−8.36 (8H, m), 7.86 (3H, br s), 7.66 (4H, d, J = 9 Hz), 7.33−7.04 (34H, m), 6.82 (4H, d, J = 9 Hz), 6.18 (4H, s), 6.04 (12H, s), 4.76 (2H, d, J = 6), 4.41 (1H, t, J = 6), 4.28−4.05 (8H, m), 3.96−3.50 (40H, m), 1.29 (36H, s). Anal. Calcd for $C_{145}H_{164}F_{24}N_4O_{17}P_4$: C = 61.87, H = 5.87, N = 1.99. Found: C = 61.65, H = 6.01, N = 1.96. Data for **2**·4PF$_6$ follow. Mp: >250 °C. LSIMS: *m*/*z* = 3205 [M − PF$_6$]$^+$, 3060 [M − 2PF$_6$]$^+$, 2915 [M − 3PF$_6$]$^+$, 2770 [M − 4PF$_6$]$^+$. ^{1}H NMR [$(CD_3)_2CO$]: δ = 9.22−9.14 (8H, m), 8.30−8.21 (8H, m), 7.96 (1H, s), 7.92 (2H, s), 7.74 (4H, d, J = 9 Hz), 7.52−7.05 (34H, m), 6.83 (4H, d, J = 9 Hz), 6.23 (4H, s), 6.13 (16H, s), 6.05 (4H, s), 4.80 (2H, d, J = 6 Hz), 4.40 (1H, t, J = 6 Hz), 4.28−4.10 (8H, m), 3.96−3.60 (72H, m), 1.29 (36H, s). Anal. Calcd for $C_{173}H_{204}F_{24}N_4O_{27}P_4$: C = 62.00, H = 6.14, N = 1.67. Found: C = 61.84, H = 6.23, N = 1.66.

Electrochemical Measurements. Cyclic voltammetry (CV) and differential pulsed voltammetry (DPV) experiments were performed in argon-purged acetonitrile solution using an EG&G Princeton Applied Research model 273 potentiometer. The working and counter electrodes for the V-shaped compound **1**$^{4+}$ were Pt with fine glass frits (0.03 cm^2) which were polished with a 0.05-μm alumina−water slurry on a felt cloth prior to use. For the rotaxanes **2**$^{4+}$ and **3**$^{4+}$, a Pt electrode was the reference electrode and a carbon electrode was the working electrode. The reference electrode was a saturated calomel electrode. The concentration was 5×10^{-4} M for **2**$^{4+}$ and **3**$^{4+}$ and 5×10^{-5} M for **1**$^{4+}$, with 0.05 M tetrabutylammonium tetrafluoroborate as the supporting electrolyte. CV experiments were performed using scan rates of 20, 50, 200, and 500 mV s^{-1}; DPV experiments were performed using scan rates of 4, 15, and 20 mV s^{-1}, pulse heights of 50 and 75 mV, and pulse widths of 40 ms. The reported peak positions were evaluated from the DPV experiments. The peak positions were calibrated by adding ferrocene (Aldrich, 98%) to the solution for the final scans. The experimental errors on the potential values were ±10 mV.

Langmuir−Blodgett Monolayers. Langmuir monolayers were prepared on aqueous subphases using an NIMA Technology type 611 Langmuir trough. The spreading solvent was THF (Acros, 99.9%) containing 0.1 mM of compound, and the water subphase was 18.2 MΩ Milli-Q water. The monolayers were prepared by adding 200 μL of solution to the subphase, which was maintained at 25 °C. Before compression, the monolayers were equilibrated for 30 min. The monolayers were initially compressed at 15 cm^2/min until the pressure (π) began to sharply increase. At that point, the compression speed was reduced to 2 cm^2/min for the remainder of each isotherm.

After the pressure−area (π−A) isotherms were obtained for each compound, Langmuir−Blodgett (LB) monolayers were deposited onto hydrophilic silicon substrates. Just prior to monolayer deposition, the silicon substrates were cleaned for 10 min at 90 °C in piranha solution, consisting of a 70:30 vol ratio of concentrated $H_2SO_{4(aq)}$/30% $H_2O_{2(aq)}$. Compact single monolayers were transferred at a rate of at 1 mm/min on the upstroke at surface pressures just below the point where the surface compressibility began to decrease: 38 mN/m (**1**$^{4+}$ and **2**$^{4+}$) and 28 mN/m (**3**$^{4+}$). The areas per molecule during the depositions were 49, 62, and 110 Å^2, with transfer ratios of 1.1, 1.1, and 1.2 for **1**$^{4+}$, **2**$^{4+}$, and **3**$^{4+}$, respectively. The uniformity of the monolayers was evaluated by atomic force microscopy (AFM) using a Topometrix Explorer in noncontact mode. Silicon probe tips were used at a resonance frequency of 190 kHz.

Device Fabrication and Transport Measurements. The devices containing **1**$^{4+}$, **2**$^{4+}$, or **3**$^{4+}$ were fabricated on ⟨100⟩ silicon wafers with a 1500-Å silicon oxide layer (WaferNet). The bottom set of electrodes were made by first patterning a photoresist on the wafer. Aluminum (1000 Å, Materials Research Corp., 99.995%) was evaporated onto the mask using an electron beam evaporator, and the electrodes were formed by liftoff. These bottom electrodes consisted of 6-μm-wide wires each connected to 0.5-mm × 0.5-mm macroscopic contact pads. Exposure to air formed a native aluminum oxide layer. A single LB monolayer of a given compound was deposited onto 3-cm-wide wafers containing multiple copies of the bottom electrodes. Finally, a top electrode set, consisting of 11-μm-wide lines connected to large pads, was deposited through a shadow mask on top of the monolayer, perpendicular to the bottom electrodes, yielding devices with 66-μm^2 active areas. This was accomplished by electron beam evaporation of Ti (50 Å, Materials Research Corp., 99.995%), Cr (200 Å, Materials Research Corp., 99.99+%), or Al. The Ti and Cr depositions were immediately followed by evaporation of Al or Au (1000 Å) through the shadow mask directly onto the monolayer. The Ti (or Cr) layer functioned as a diffusion barrier to Al or Au to prevent shorting the devices. Active devices were formed at the intersections of the top and bottom electrodes, a cross section of which is depicted in Figure 3A. The thickness of the Al_2O_3 tunnel barrier was estimated by preparing devices without including a molecular monolayer (only the metal electrodes) and modeling the measured I−V characteristics of those junctions as a metal/insulator/metal (MIM) diode.[17] A tunnel barrier thickness of approximately ∼1 nm was calculated.

Control devices were fabricated in a similar fashion, except that eicosanoic acid monolayers were substituted for the monolayers of **1**$^{4+}$, **2**$^{4+}$, or **3**$^{4+}$. The subphase for the monolayers was 1 mM $CdCl_{2(aq)}$, which was adjusted to pH 6.8 by addition of NaOH immediately prior to use. Such a subphase has been previously demonstrated to produce nearly defect-free LB films of long-chain carboxylic acid amphiphiles.[18] The monolayers were spread onto the subphase by adding 130 μL of chloroform containing 1 mM eicosanoic acid. The monolayers were compressed at 2 cm^2/min to a pressure of 30 mN/m and an area per molecule of 20 Å^2. They were deposited as LB films onto the bottom electrode set on the upstroke at 1 mm/min. The transfer ratio for the deposition was 1.0.

All transport measurements were performed in air and at room temperature. A micromanipulator probe station (Microprobe) enclosed in a Faraday cage was used to make electrical contact to the macroscopic contact pads. Current vs voltage (I−V) curves from the devices were obtained by grounding the top electrode (V) while applying a bias voltage to the bottom electrode (I), as depicted in Figure 3A. For the purposes of discussion, forward bias refers to application of a negative potential to the bottom electrode, while reverse bias corresponds to applying a positive bias. The output current from the ground was measured using a DL Instruments Model 1211 current preamplifier.

Results

Synthesis and Characterization. Reaction of 3,5-bis(bromomethyl)benzyl alcohol (**4**) with 4,4′-bipyridine (**5**), followed

(17) Simmons, J. G. *J. Appl. Phys.* **1963**, *34*, 2581−2590.

(18) (a) Honig, E. P.; Hengst, J. H. Th.; Den Engelsen, D. *J. Colloid Interface Sci.* **1972**, *45*, 92−102. (b) Claesson, Per M.; Berg, J. M. *Thin Solid Films* **1989**, *176*, 157−164.

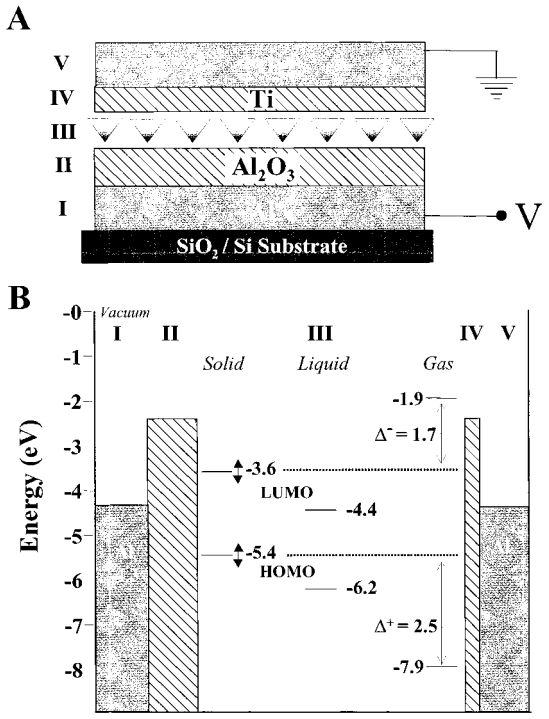

Figure 3. (a) Side view cross section of device junctions. (b) Energy level diagram of the device shown in (a). The Fermi levels of the Al electrodes are shown at both ends of the diagram. The diagonally striped areas between the electrodes and the rotaxane energy levels are tunneling barriers. The thick barrier is the Al_2O_3 passivating layer, and the thin barrier is the Ti/molecule interface. The device conduction states are in the middle along with the solution-state molecular levels and calculated gas-phase levels. The solution-state levels were determined from $E_{SCE} = -4.842$ eV with respect to a zero vacuum level.

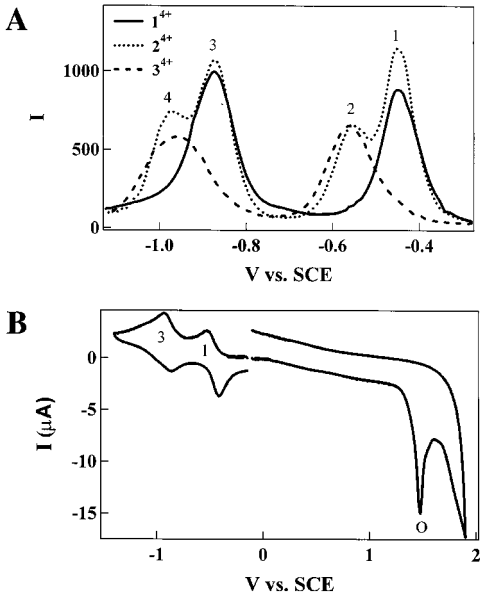

Figure 4. (a) Differential pulsed voltammetry scans of $\mathbf{1}^{4+}$, $\mathbf{2}^{4+}$, and $\mathbf{3}^{4+}$. The vertical axis is in units of relative current, while the horizontal axis is plotted relative to SCE. (b) Cyclic voltammograms (500 mV/s) of $\mathbf{1}^{4+}$.

by counterion exchange, afforded the bis(hexafluorophosphate) salt **6**·2PF_6 in a yield of 92%. Alkylation of **6**·2PF_6 with the tetraarylmethane-based chloride **7** gave the V-shaped compound **1**·4PF_6 in a yield of 97%, after counterion exchange. Heating a solution of **7**·4PF_6 and 19 equiv of bis-*p*-phenylene-34-crown-10 (**8**) afforded the [2]rotaxane **2**·4PF_6 and the [3]rotaxane **3**·4PF_6, which were separated by column chromatography and isolated in yields of 14 and 52%, respectively. The remaining V-shaped compound **1**·4PF_6 (ca. 34%) was recovered unchanged after column chromatography. The liquid secondary ion mass spectra of the V-shaped compound **1**·4PF_6 and of the rotaxanes **2**·4PF_6 and **3**·4PF_6 revealed peaks at *m*/*z* values for $[M - PF_6]^+$, $[M - 2PF_6]^+$, $[M - 3PF_6]^+$, and $[M - 4PF_6]^+$ corresponding to the consecutive losses of the hexafluorophosphate counterions. The ^{1}H NMR spectrum [$(CD_3)_2CO$, 25 °C] of the V-shaped compound **1**·4PF_6 revealed two sets of signals (δ 9.44 and 9.38) for the α-bipyridinium protons. One of these sets of resonances corresponds to the α-bipyridinium protons adjacent to the "terminal" tetraarylmethane-based stoppers. The other set is associated with the α-bipyridinium protons next to the "central" 3,5-disubstituted benzyl ring. In solution, the macrocyclic component of the [2]rotaxane **2**·4PF_6 shuttles[19−21] along the linear portion of the V-shaped component from one bipyridinium recognition site to the other. This dynamic process is fast [$(CD_3)_2CO$, 25 °C] on the ^{1}H NMR time scale. Thus, the "encircled" and "free" bipyridinium units cannot be distinguished. In this [2]rotaxane, the two sets of α-bipyridinium protons resonate at the same chemical shift (δ 9.28). By contrast, in the case of the [3]rotaxane **3**·4PF_6, two partially overlapping sets of signals (δ 9.22−9.14) are observed for these protons. For both rotaxanes, however, the resonances associated with the α-bipyridinium protons are shifted (ca. −0.2 ppm) relative to those observed for the same protons in the "free" V-shaped compound **1**·4PF_6. These chemical shift changes are a result of shielding effects exerted by the 1,4-dioxybenzene rings of the macrocyclic component(s) on the α-bipyridinium protons of the V-shaped component.

Electrochemical Measurements. The electrochemical properties of $\mathbf{1}^{4+}$, $\mathbf{2}^{4+}$, and $\mathbf{3}^{4+}$ closely resemble those of their triply branched cousins.[10c] That is, reduction processes associated with the bipyridinium-like units are reversible, whereas oxidation of the compounds is irreversible. In addition, electron-donor interactions between the bipyridinium units and crown ether macrocycles increase the reduction potentials of the bipyridinium units. In Figure 4A we present the reduction DPV scans for the compounds used in these studies. The V-shaped molecule $\mathbf{1}^{4+}$ shows two reversible bielectronic reduction waves at −0.45 (peak 1) and −0.87 V (peak 3). Peak 1 is associated with the first one-electron reduction of each bipyridinium unit, and peak

(19) For a description of the first degenerate "molecular shuttle", see: Anelli, P.-L.; Spencer, N.; Stoddart, J. F. *J. Am. Chem. Soc.* **1991**, *113*, 5131−5133.

(20) For examples of chemically, electrochemically, and/or photochemically controllable molecular shuttles, see: (a) Bissell, R. A.; Córdova, E.; Kaifer, A. E.; Stoddart, J. F. *Nature* **1994**, *369*, 133−137. (b) Martínez-Díaz, M.-V.; Spencer, N.; Stoddart, J. F. *Angew. Chem., Int. Ed. Engl.* **1997**, *36*, 1904−1907. (c) Murakami, H.; Kawabuchi, A.; Kotoo, K.; Kunitake, M.; Nakashima, N. *J. Am. Chem. Soc.* **1997**, *119*, 7605−7606. (d) Ashton, P. R.; Ballardini, R.; Balzani, V.; Baxter, I.; Credi, A.; Fyfe, M. C. T.; Gandolfi, M. T.; Gómez-López, M.; Martínez-Díaz, M.-V.; Piersanti, A.; Spencer, N.; Stoddart, J. F.; Venturi, M.; White, A. J. P.; Williams, D. J. *J. Am. Chem. Soc.* **1998**, *120*, 11932−11942. (e) Armaroli, N.; Balzani, V.; Collin, J.-P.; Gaviña, P.; Sauvage, J.-P.; Ventura, B. *J. Am. Chem. Soc.* **1999**, *121*, 4397−4408. (f) Collin, J.-P.; Gaviña, P.; Sauvage, J.-P. *New J. Chem.* **1999**, *21*, 525−528. (g) Ballardini, R.; Balzani, V.; Dehaen, W.; Dell'Erba, A.; Raymo, F. M.; Stoddart, J. F.; Venturi, M. *Eur. J. Org. Chem.* **1999**, 591−602.

(21) For reviews on molecular machines, see: (a) Stoddart, J. F. *Chem. Aust.* **1992**, *59*, 576−577 and 581. (b) Gómez-López, M.; Preece, J. A.; Stoddart, J. F. *Nanotechnology* **1996**, *7*, 183−192. (c) Balzani, V.; Gómez-López, M.; Stoddart, J. F. *Acc. Chem. Res.* **1998**, *31*, 405−414. (d) Sauvage, J.-P. *Acc. Chem. Res.* **1998**, *31*, 611−619. (e) Chambron, J.-C.; Sauvage, J.-P. *Chem. Eur. J.* **1998**, *4*, 1362−1366. (f) Kaifer, A. E. *Acc. Chem. Res.* **1999**, *32*, 62−71. (g) Leigh, D. A.; Murphy, A. *Chem. Ind.* **1999**, 178−183.

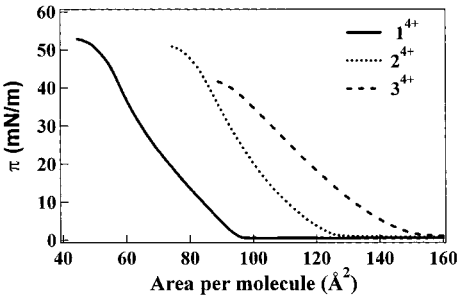

Figure 5. Pressure (π) vs area per molecule isotherms of $\mathbf{1}^{4+}$, $\mathbf{2}^{4+}$, and $\mathbf{3}^{4+}$.

3 corresponds to the second reduction. Molecule $\mathbf{2}^{4+}$ exhibits four reversible one-electron reduction waves at −0.45 (peak 1), −0.55 (peak 2), −0.89 (peak 3), and −0.97 V (peak 4). The interaction of the single crown ether macrocycle with one of the bipyridinium units shifts its reduction potentials to more negative voltages. Thus, peak 1 arises from the first reduction of the free bipyridinium unit and peak 2 from initial reduction of the bipyridinium unit encircled by the macrocycle. A second reduction of the free bipyridinium unit results in peak 3, while the second reduction of the bipyridinium unit encircled by the macrocycle gives peak 4. Molecule $\mathbf{3}^{4+}$ has two bielectronic waves at −0.56 (peak 2) and −0.97 V (peak 4). These are similar to peaks 1 and 3 observed for $\mathbf{1}^{4+}$, except the first and second reductions of each bipyridinium unit have been shifted to more negative voltages due to interaction with the macrocycles.

Cyclic voltammograms for compound $\mathbf{1}^{4+}$ are shown in Figure 4B. The scan to negative potentials demonstrates the reversible nature of the reduction waves. First, the cathodic and anodic waves are of equal intensities; second, the peaks are separated by only 60 mV; third, the peak positions are independent of scan rate. In scans to positive potentials the irreversible nature of the oxidation can be inferred from the absence of a cathodic peak associated with the anodic wave at peak O. According to DPV measurements, oxidation processes begin to occur at ∼+1.4 V for all three molecules. Specific assignments to the oxidation peaks are precluded because of their irreversibility.

Force Microscopy Characterization of Langmuir−Blodgett Monolayers. Surface pressure (π) vs area (per molecule) isotherms for monolayers made from each compound are plotted in Figure 5. The effect of adding one or two rings to the backbone is to increase the area at which the molecules begin to interact with each other on the trough, as detected by the sharp increase in π: 96, 128, and 155 Å^2/mol for $\mathbf{1}^{4+}$, $\mathbf{2}^{4+}$, and $\mathbf{3}^{4+}$, respectively. Aside from the area offset, the isotherms for $\mathbf{1}^{4+}$ and $\mathbf{2}^{4+}$ monolayers are similar and show complete collapse by ∼50 mN/m. The most pronounced effect occurs when the second ring is added: the collapse pressure decreases by about 10 mN/m. Presumably, the addition of the rings increases the separation between branches and destabilizes the monolayers at lower surface pressures. The rings may also affect the tilt angle of the principal molecular axis with respect to the substrate normal. These changes can affect the measured device properties, as will be discussed below.

LB monolayers deposited on hydrophilic substrates are oriented with the hydrophilic hydroxyl groups toward the surface and the tetraarylmethane-based stoppers away from the surface. Simple wetting tests verified this orientation: after deposition of a single monolayer, the initially hydrophilic substrates were rendered hydrophobic. Deposition of a second monolayer would yield a hydrophilic surface. This was also the case for monolayers deposited onto electrodes. These results are consistent with those found by others, who made LB monolayers from similar rotaxanes containing three instead of two branches.[10c] The AFM surface topography image in Figure 6 shows that the monolayers are uniform. Over a 1-μm^2 scan area, the root-mean-square roughness for these films was typically measured to be only 0.8 Å, with an average peak-to-valley height of 2 Å. These height variations are very small (10%) compared to the overall length of the fully extended molecules (∼20 Å). Although not observed by AFM, the presence of bilayers and pinhole defects cannot be ruled out. The transfer ratios of 1.1−1.2 suggest that there should be regions of local bilayer or multilayer formation. However, these types of defects should not seriously degrade device performance in the same manner as pinholes, which would short-circuit the devices. As will be discussed below, short-circuited devices were not found unless the Ti buffer layer was omitted from device fabrication. This suggests either that pinholes were not present in our final devices or that Ti induced pinhole closure. While a pinhole-free monolayer could explain the absence of short circuits, the small device areas (66 μm^2) could also account for pinhole-free devices, as has been found previously.[6d]

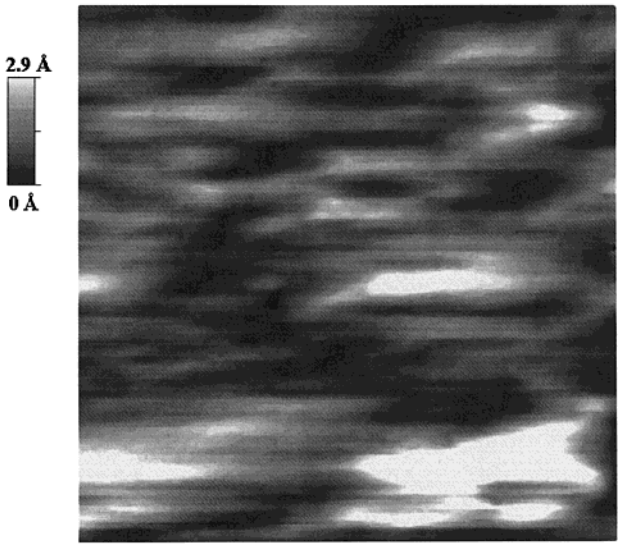

Figure 6. AFM topography image of a $\mathbf{1}^{4+}$ LB monolayer on a silicon substrate. The scan size is 1 μm.

Device Properties: Fabrication Yield, Transport Characteristics, and Aging. The most common mode of failure for sandwich-type devices is a short circuit between the top and bottom electrodes. For our initial devices, such shorts lowered our device yield to below 50%. However, the vast majority of those short circuits arose from improper handling of the devices, not from the fabrication process, and the eventual device yield was effectively 100%. Out of approximately 100 devices measured, no defective devices were found. Direct evaporation of aluminum onto the molecular monolayer degraded the monolayer, leading to short-circuited devices. However, the use of either Ti or Cr for the top electrodes produced good devices. Ti, in particular, is known to form a uniform wetting layer on organic films, where it most likely forms a conducting TiC_x interface.[22] Such an interface would be expected to form via reaction of Ti with the bulky phenyl groups at the hydrophobic end of the molecule, since it is that end that faces away from the bottom electrode. As we show below, the electrochemical properties of the molecules in solution are largely retained in

(22) (a) Konstantine, K.; Zhang, P.; Opila, R. L.; Allara, D. L. *Surf. Sci.* **1995**, *338*, 300−312.

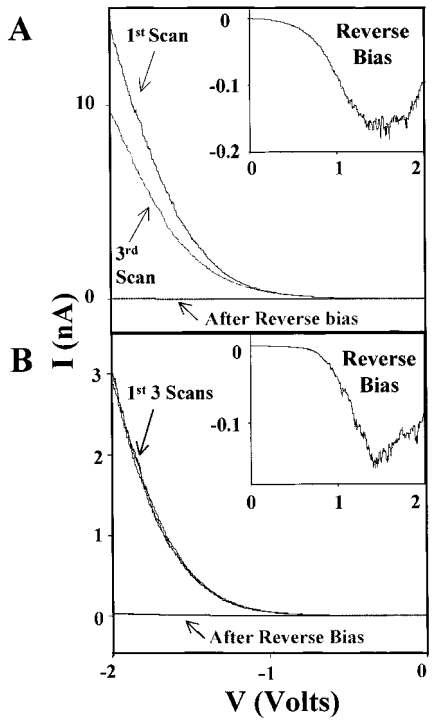

Figure 7. (a) $I-V$ curves for $\mathbf{3}^{4+}$ devices, showing a fresh device: read, read third time, write, read. (b) $I-V$ curves for $\mathbf{3}^{4+}$ devices 30 h old, read 3 times (no change), write, read.

the solid state. Apparently, the protected bipyridinium units remain intact after deposition of the Ti film. An Al layer was subsequently evaporated directly on top of the Ti electrode. Current/voltage traces for devices made from $\mathbf{3}^{4+}$ monolayers are displayed in Figure 7. Similar voltage traces for the $\mathbf{2}^{4+}$-based devices were reported previously.[23] These devices, initially probed at forward bias (negative) voltages, all show a markedly nonlinear current increase with applied voltage (Figure 7A, "1st scan"). Subsequent scans yield slightly lower (~20% less) current levels (Figure 7A, "3rd scan"), but further measurements at negative bias remain stable. A reverse bias scan (Figure 7A, "reverse bias" trace) is characterized by a reduced current level as well as a hump in the $I-V$ curve between 1.15 and 1.4 V, depending on the device. Significantly, measurements made after a positive bias above +0.7 V was applied show a pronounced decrease in current for both reverse and forward biases (Figure 7A, "after reverse bias" trace). At −1.6 V, the current decreases irreversibly by a factor of 60−80 after a reverse bias scan. Here we have the basis for a singly configurable, molecular switch that is initially "closed" (high current flow) and then, after reverse biasing, "open" (low current flow). The "open" and "closed" states of the switch are read at forward bias voltages, which do not perturb the molecules. The configurability of our junctions was recently exploited to make logic gates from parallel arrays of our molecular-based devices.[23]

The aging characteristics of our devices exhibited a strong dependence on the monolayer species (Figure 7B). Devices constructed from $\mathbf{3}^{4+}$ continued to exhibit switching behavior for several days after device fabrication, but we observed a factor of 3 drop in the overall magnitude of current within 24−40 h of device preparation. In addition, an initial forward scan of an "aged" device did not effect the device characteristics (Figure 7B, "1st 3 scans"). Devices fabricated from $\mathbf{1}^{4+}$ and $\mathbf{2}^{4+}$ monolayers exhibited similar decay characteristics, although with different time constants. For the $\mathbf{1}^{4+}$ device, the time constant was approximately 1 week, and for the $\mathbf{2}^{4+}$ device, the time constant was 2−3 days. Possible chemical mechanisms responsible for device aging will be discussed below.

Discussion

Resonant Tunneling through Molecular States. The solid-state device $I-V$ behavior can be understood in terms of the molecular properties observed in solution. Current flow in both the solid-state devices and the solutions is reversible at negative and irreversible at positive potentials. This correspondence between the solution and solid-state results suggests that the fundamental molecular, electronic properties are retained in the solid-state devices. If this is the case, then the forward bias current flow should be determined by the LUMO states, whereas the reverse bias current should be mediated by the HOMO states. As with the solution-phase voltammetry, the irreversible reverse bias hump in the solid-state $I-V$ curves should correspond to oxidation of the molecules, thereby decreasing the tunneling current to a minimum when all of the molecules are oxidized. The irreversible oxidation of similar molecules in solution has been previously documented[10c,11a] and is one reason that these compounds were used here. Thus, oxidation is a plausible mechanism by which the junctions are opened.

Better insight into how the junctions operate can be gained by plotting $I-V$ traces as normalized conductance [dI/dV (V/I)], which, under conditions of low current flow (for our case, this is ~1 aA/molecule), represents the normalized density of states (NDOS).[24] When the switches are closed, the NDOS at negative voltages is resolved into two features. In Figure 8A, we present such plots for each of the three devices based on $\mathbf{1}^{4+}$, $\mathbf{2}^{4+}$, and $\mathbf{3}^{4+}$. The first broad peak indicates the presence of conduction levels, E_c, at ~ −0.7 V and is plotted at −3.6 eV relative to the vacuum level at 0 eV. We believe that the onset of high current arises from resonant tunneling through these states, and that these states correspond to the solution-phase LUMO obtained from the first reduction of the bipyridinium units (−4.4 eV in Figure 3B). As mentioned above, current flow through these devices decreases slightly to some stable value after an initial forward scan. In Figure 8B, we present the NDOS of devices that have been "burned in" by a few of these scans. The relative intensity of the first NDOS peaks is decreased, indicating that some of the molecules in the junction are no longer able to provide a resonant tunneling pathway for current flow.

In Figure 8C, we present the NDOS for the reverse bias scans—again for all three devices. The NDOS has a peak at 0.7, 0.8, and 0.9 V for the $\mathbf{3}^{4+}$, $\mathbf{2}^{4+}$, and $\mathbf{1}^{4+}$ devices, respectively. Above +1.4 V, the $I-V$ scans in Figure 6A,B show a substantial drop in current. Since these scans are not reversible, it is difficult to precisely locate the position of the valence states, E_v, responsible for the tunneling current. However, they should lie somewhere between the peaks in the NDOS and the hump in the $I-V$ curves. The average value is used for the solid-state valence level, which is plotted at −5.4 eV (Figure 3B), along with the associated solution state HOMO, at −6.2 eV, obtained from solution-phase voltammetry, where $E_{SCE} = -4.842$ eV with respect to the zero vacuum level was used. These states are associated with the phenoxy subunits. Subsequent positive voltage scans reveal a featureless current/voltage trace with no peaks in the NDOS, and such scans can be understood using

(23) Collier, C. P.; Wong, E. W.; Behloradský, M.; Raymo, F. M.; Stoddart, J. F.; Kuekes, P. J.; Williams, R. S.; Heath, J. R. *Science* **1999**, *285*, 391−394.

(24) Feenstra, R. M.; Stroscio, J. A.; Fein, A. P. *Surf. Sci.* **1987**, *181*, 295−306.

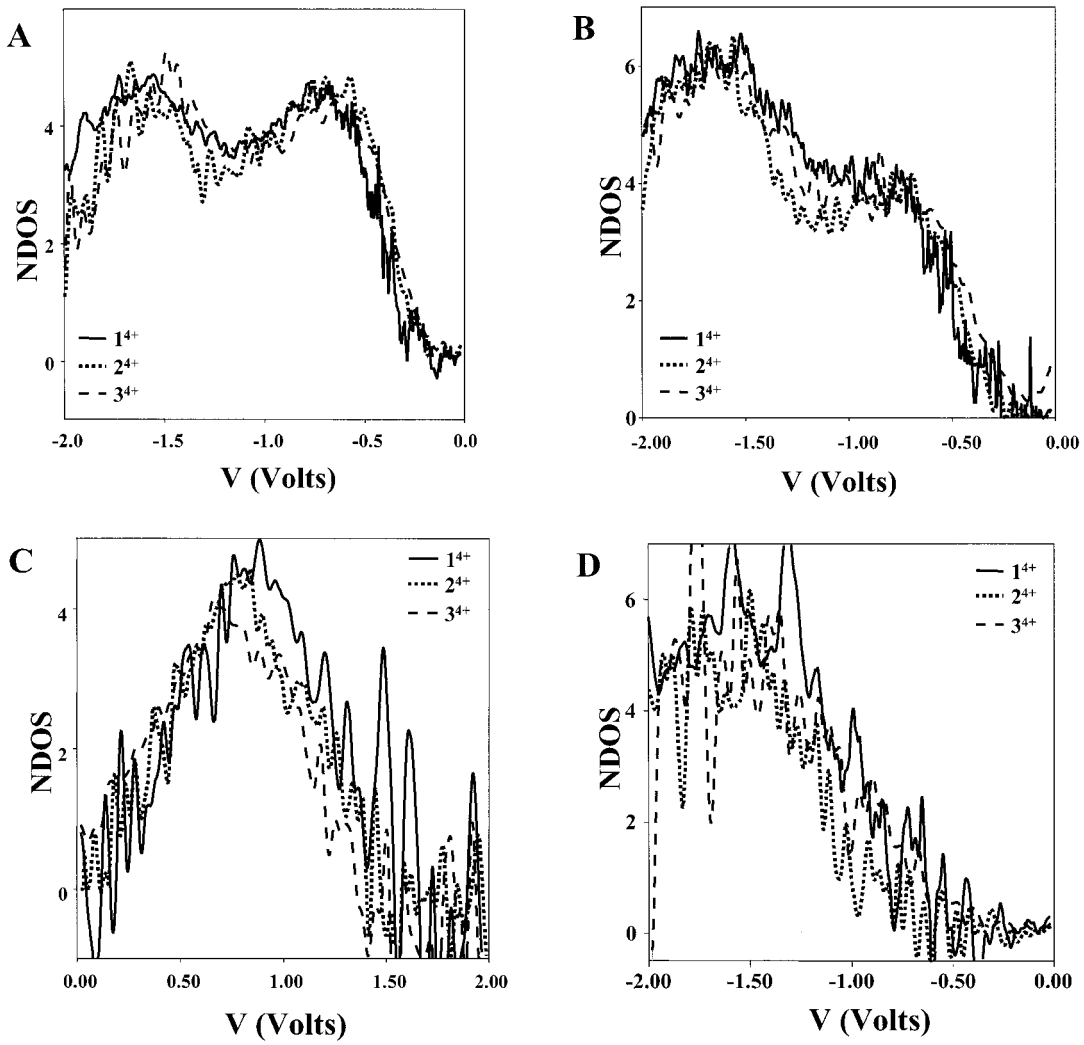

Figure 8. (a) NDOS curves for $\mathbf{1}^{4+}$, $\mathbf{2}^{4+}$, and $\mathbf{3}^{4+}$. (b) NDOS for stabilized devices. (c) NDOS for reverse bias scan. (d) NDOS curves showing open switch.

nonresonant tunneling models. Similar results are found in the solution-phase voltammetry, in which these molecules are destroyed by oxidation.

Reverse biasing the junction effectively "opens" the switch, presumably by removing resonant tunneling mechanisms that were provided by the molecules. Further support for this conclusion is found by comparing the NDOS of closed and open devices (Figure 8A,D). The notable difference is that the first NDOS peak present in the closed device disappears in the open device. The NDOS of these open devices appears very similar to those of the control devices fabricated from eicosanoic acid. Thus, reverse biasing the devices (Figure 8C) removes the molecular levels from participating in resonant tunneling, dramatically reducing the currents. At voltages more negative than −1.5 V, we believe the device properties are not strongly correlated with the electronic properties of the molecular junctions. We reach this conclusion because the simple linear amphiphile tunneling junctions employed as control devices exhibit similar behavior in this voltage range. In solid-state devices, similar behavior is observed at high voltages when the device enters what is known as the Fowler−Nordheim regime,[25] where the tunnel barrier width becomes dependent upon the applied voltage.

We have suggested that the molecular states are responsible for the resonant tunneling observed in our devices, and that oxidation of the molecules opens the junctions. This connection can be seen more clearly by closely comparing the solution-phase and solid-state results. Assigning energies with respect to an absolute vacuum level is difficult,[26] especially when trying to infer the solid-state energies from molecular states in solution. It is apparent from Figure 3B that the solid-state E_c and E_v levels are both shifted by +0.8 eV with respect to the solution-phase HOMO−LUMOs; however, this uniform shift is probably coincidence, as will be apparent in the discussion that follows. The connection between the solid-phase and solution-phase electronic levels can be made more concrete by first estimating ionization potentials from the DPV results. There are a number of empirical correlations between the oxidation half-wave potentials, $E_{1/2}$, and the ionization potentials, I_g, of organic molecules.[27] Of course, different choices of compounds included in the correlation fits can increase the calculated I_g by a few tenths of an electronvolt, but this will not alter the discussion that follows. Using 1.4 eV in the relation $I_g = 5.832 + 1.442E_{1/2}$ (SCE), obtained using a broad selection of different compounds,[27b]

(25) Sze, S. M. *The Physics of Semiconductor Devices*; Wiley: New York, 1981.

(26) Ishii, H.; Sugiyama, K.; Ito, E.; Seki, K. *Adv. Mater.* **1999**, *11*, 605−625.

(27) (a) Miller, L. L.; Nordblom, G. D.; Mayeda, E. A. *J. Org. Chem.* **1972**, *37*, 916−918. (b) Seki, K. *Mol. Cryst. Liq. Cryst.* **1989**, *171*, 255−270.

gives an ionization potential of 7.9 eV for an isolated rotaxane. This calculated value compares well with the experimental I_g, 8.0 eV,[27a] for anisole, which closely resembles the phenoxy functionality associated with the rotaxane HOMO states responsible for the irreversible oxidation of the rotaxanes in solution. Similarly, the electron affinity A_g can be calculated from the half-wave reduction potentials using the empirical relation $A_g = 0.81E_{1/2} + 2.22$ (SCE).[28] For the LUMO corresponding to the first reduction of the bipyridiniums, $A_g(-0.45\ V) = 1.9$ eV. It should be noted that other empirical relationships could increase the A_g by a few tenths of an electronvolt,[29] but, again, this will not affect the salient conclusions.

For organic molecules in the solid state, electronic polarization of the surrounding molecules shifts the positions of the ionized states responsible for conduction.[30] The polarization energies P^+ and P^- determine the position of the solid-state conduction states according to $E_c = A_g - P^-$ and $E_v = I_g + P^+$.[30] Polarization energies have been experimentally determined to be 1.7 eV for a variety of compounds and can range from 0.9 to 3.0 eV.[30c] For our systems, the differences between the calculated gas-phase and experimental solid-state energies are defined by $\Delta^- = A_g - E_c$ and $\Delta^+ = E_v - I_g$. The values $\Delta^- = 1.7$ eV and $\Delta^+ = 2.5$ eV (Figure 3b) are within the range expected for the polarization energy of organic molecules. It is often assumed that $P^- = P^+$, but this is only true for molecules without a permanent quadrupole moment, such as benzene. Otherwise, $P^+ > P^-$, and for several organic molecules P^+/P^- can range between 1.4 and 1.6.[30b] The rotaxanes in our studies should have permanent quadrupole moments. The ratio $\Delta^-/\Delta^+ \approx 1.5$ is consistent with the results from other compounds and suggests that our Δ values correspond to the polarization energies. Therefore, the HOMO−LUMO states determined in solution can be correlated to the conduction states in our devices. While there is no mechanistic information about the irreversible switching of the devices, the close correspondence between the device tunneling states and the molecular states observed in solution leads to the conclusion that oxidation of the molecules is a reasonable explanation.

It should be noted that it highly possible that other factors, in addition to the polarization energies, contribute to the Δ values. The polarization energies determined for other compounds were for evaporated thin films.[30b,c] For monolayers, the polarization energy could be altered by the orientational ordering or by the lack of molecules above and below the monolayer. Additionally, dipole layers induced at the electrode/molecule interfaces may raise or lower the states. Finally, induced image charges in the more proximal top electrode will certainly bring the HOMO−LUMO states closer together.[25]

The fact that all three molecules exhibited similar behavior argues that the V-shaped backbone, rather than mechanical motion of the crown ether rings, dominates the electronic properties of the junction. If molecular mechanical motions are occurring in the $\mathbf{2}^{4+}$- and $\mathbf{3}^{4+}$-based devices, then the electronic signatures of that motion are not obvious from our measurements. However, the shuttling of the macrocyclic component from one bipyridinium recognition site to the other in the [2]-rotaxane $\mathbf{2}^{4+}$ is fast (vide supra) on the ^{1}H NMR time scale in solution at ambient temperature. Thus, the "encircled" and "free" bipyridinium units of $\mathbf{2}^{4+}$ cannot be distinguished in the ^{1}H NMR spectrum recorded under these conditions. By contrast, the "encircled" and "free" bipyridinium units of $\mathbf{2}^{4+}$ give rise to distinct peaks (Figure 4A) in the differential pulse voltammogram. These observations indicate that the shuttling process is slow on the time scale of the electrochemical experiment performed in solution. It must be noted that this dynamic process exchanges two degenerate co-conformations that are indistinguishable from each other.

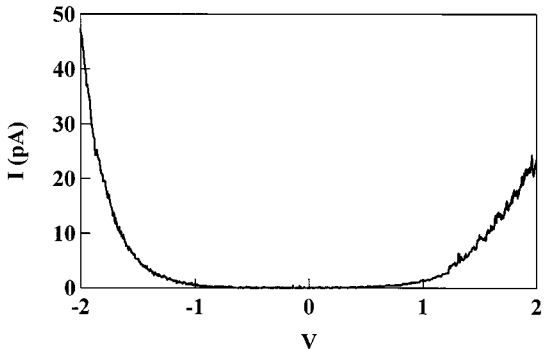

Figure 9. $I-V$ curve for eicosanoic acid-based device.

Lipid Control Devices. The $I-V$ characteristics of the lipid control devices were investigated to better understand the rotaxane-based switches. As with previous measurements,[8] the $I-V$ curves from the lipid devices displayed symmetric nonresonant tunneling behavior between ± 1 V as well as a $\sim$5-fold decrease in current after aging for a day. At voltages higher than ± 1 V, the $I-V$ curves for the day-old devices are asymmetric, with currents of 20 nA at $+2$ V and 40 nA at -2 V (Figure 9). The asymmetry is somewhat greater than that found for Al−lipid−Al devices made by others. This asymmetry would arise if the potential barrier at the top interface were smaller than that of the bottom interface. This is entirely likely since the top electrode is evaporated and has Ti in addition to Al. A similar slight asymmetry favoring the forward bias current was observed for all of the opened rotaxane-based devices. The junction resistance in the lipid devices could also be increased by applying a positive voltage, presumably by oxidation of the Ti electrode. However, the effect is significantly less pronounced than that in the rotaxane-based devices. Only after oxidation at $+2$ V for >10 min did the resistance decrease by a factor of 20, as measured at -2 V. Finally, the negative bias NDOS curves for unoxidized lipid devices resemble those of the oxidized rotaxane devices; that is, they increase monotonically at negative bias without any peak. The absence of a peak is consistent with nonresonant tunneling and further corroborates the conclusion that current flow in the unwritten rotaxane devices occurs by resonant tunneling.

Conclusion

Amphiphilic [*n*]rotaxanes incorporating redox-active units in one of their components can be synthesized efficiently using a thermodynamically controlled self-assembly process—the so-called slippage approach. These molecules are composed of a bipyridinium-based V-shaped component, encircled by one or two macrocycles. Two hydrophobic tetraarylmethane-based stoppers at the ends of the V-shaped component and a hydrophilic hydroxymethyl group at the junction of its two arms impose amphiphilic character on these molecules. By employing these two rotaxanes and their V-shaped component in its free form, we have fabricated switchable, molecule-based devices

(28) Loutfy, R. O.; Hsiao, C. K.; Ong, B. S.; Keoshkerian, B. *Can. J. Chem.* **1984**, *62*, 1877−1885.

(29) Chen, E. C. M.; Wentworth, W. E. *Mol. Cryst. Liq. Cryst.* **1989**, *171*, 271−285.

(30) (a) Silinsh, E. A. *Organic Molecular Crystals*; Springer-Verlag: Heidelberg, 1980. (b) Sato, N.; Seki, K.; Inokuchi, H. *J. Chem. Soc., Faraday Trans. 2* **1981**, *77*, 1621−1633. (c) Sato, N.; Inokuchi, H.; Silinsh, E. A. *Chem. Phys.* **1987**, *115*, 269−277.

that have been used to make singly configurable logic gates.[23] Careful design of molecular structure enables integration of molecules into solid-state devices while retaining the molecular electronic properties desired in the device. Since the present devices are only singly switchable, a clear goal now is to make a reversibly switchable device that can be used as random access memory. Fortunately, a virtue of our fabrication process is that it is simple, allowing facile screening of molecules for potentially useful electronic properties. One possibility will be to design molecules that can undergo mechanical transformations in the solid state, analogous to rotaxanes in solution. Another challenge will be to scale down the device size and eventually incorporate molecular-scale wires such as carbon nanotubes. The similarity of the electronic behavior of the molecules in the solid-state devices to that of molecules in a dilute solution suggests that the device properties are determined largely by molecular properties. Thus, the devices should scale down to molecular dimensions without altering their fundamental properties. The devices presented here provide a compelling argument that molecular switch devices show promise in future technologies.

Acknowledgment. This research was supported by the North Atlantic Treaty Organization (Collaborative Research Grant No. 960659), the National Science Foundation, and the Defense Advanced Research Projects Agency. We acknowledge helpful discussions with Dr. Stan Williams and Dr. Sang-Ho Kim.

JA993890V